Journal of Physics: Conference Series **75** (2007) 012021 doi:10.1088/1742-6596/75/1/012021

Analysis of the experimental and computational flow characteristics with respect to the augmented lift phenomenon caused by blade rotation

R.P.J.O.M. van Rooij and E.A. Arens

Delft University Wind Energy Research Institute, Kluyverweg 1, 2629 HS Delft, The Netherlands

R.P.J.O.M.vanRooij@TUDelft.nl,

Abstract. This article focuses on the augmented lift phenomenon as a result of blade rotation in the steady state non-yawed condition. In the investigations a full Navier Stokes code FLUENT is used instead of engineering models. The calculations are compared with the measurements of the Unsteady Aerodynamic Experiment at the NASA Ames wind tunnel at wind speeds between 8m/s and 15m/s in steps of 1m/s. The computations show good agreement for the pressure distributions for almost all five segments at wind speeds below 10m/s, only large deviations occur at segment r/R= 0.47. Beyond 10m/s deviations with the experiment increase but still, apart from the inboard r/R= 0.30 segment and occasionally the r/R= 0.47 location, the results are surprisingly good. Large separated areas and cross flows dominate the flow on the suction side as can be distracted from the calculated limited streamlines. Integration to the normal force coefficient showed that the trends of the experimental data are followed reasonably well for each span section. The presence of augmented lift and stall delay was confirmed for the span sections at r/R= 0.30 and r/R= 0.47.

Nomenclature

C_d	=	segment drag force coefficient
C_n	=	segment normal force coefficient
C_l	=	segment lift force coefficient
C_p	=	pressure coefficient
c	=	chord
c/r	=	local solidity
r/R	=	span location
R	=	rotor radius
$2D$	=	2-dimensional configuration
$3D$	=	3-dimensional configuration

1. Introduction

The design of blades is often carried out with help of the Blade Element Momentum (BEM) theory and the blade is then divided in segments ranging from inboard, mid-span, outboard and tip elements. Accurate aerodynamic description of the local segment characteristics is eminent to obtain an optimal blade design. This is not only important with respect to rotor power performances but also blade loads. Use of ordinary 2D aerodynamic characteristics falls short due to rotational influences which lead to

an increase in segment lift. This behavior varies over the blade and the augmented lift reduces towards the tip. These effects have been studied by many and led to several engineering models for adjusting span-wise 2d aerodynamic lift, and is sometimes accompanied with adjustments in drag [1, 2, 3, 4]. The general trend is covered by these methods with c/r as most important tuning parameter. Detailed information of the flow around the airfoil is still rather unclear and here computational fluid dynamics (CFD) could help.

Aerodynamic CFD analyses with the Unsteady Aerodynamics Experiment (UAE, [5]) Phase VI as reference have already been carried out before, but these investigations focused on wide range of configurations for several wind speeds [6, 7, 8, 9, 10]. The present investigations zoom, in particular, into characteristics just beyond maximum lift in 2D stall where rotational effects lead to strong augmented lift (or normal force). Therefore wind speeds are selected between 8m/s and 15m/s from the steady state non-yawed configuration. A step of 1m/s is chosen to obtain the best detailed information. The comparison with the commercial code FLUENT will demonstrate how well the five different span-wise sections are estimated and this could provide opportunities to extend the research to more geometric blade designs and parameter investigations with the flow behavior as background.

2. Method

The analysis starts with the lowest tunnel velocity where the flow is almost fully attached and fluctuations of the segment pressure distributions are small. At increasing tunnel speed the segments run into the stalled condition and separated flows become dominant. Segment pressure distributions exhibit strong fluctuations and the flows over the airfoil are no longer steady. This unsteady flow behavior is simulated in the CFD computations and for 12m/s and higher steady and unsteady computations are carried out.

In the investigation the configuration of the Phase VI rotor without flow probes was chosen to avoid unnecessary disturbances. The rotor in the experiment is two bladed with a diameter of 10.058m and has one airfoil; the S809 (relative thickness 21%). The blade has taper with a maximum chord of 0.735m and a tip chord of 0.061m. The twist between r/R= 0.30 and r/R=0.95 is 15.8 deg, while the overall twist is 22.5 deg. One blade of the rotor is instrumented with electronic pressure transducers (from PSI) and are connected to 5 span-wise positions equipped with pressure orifices at r/R= 0.3, 0.47, 0.63, 0.80 and 0.95. The blade pitch angle in the series is set at 3 deg. towards feather relative to the rotor plane. The operational conditions given by the UAE S-series are given in table 1 and this data is input for the CFD calculations.

Cases	Wind speed ($m\ s^{-1}$)	Density ($kg\ m^{-3}$)	Static pressure ($N\ m^{-2}$)	Rotational speed ($rad\ s^{-1}$)	Viscosity $\times 10^5$ ($kg\ m^{-1}\ s^{-1}$)	CFD solver
S080000	8.049	1.2429	101935	7.544	1.769	steady
S090000	9.013	1.2457	101937	7.554	1.769	steady
S100000	10.051	1.2458	101890	7.555	1.769	steady
S110000	11.036	1.2285	101493	7.555	1.773	steady
S120000	12.059	1.2271	101470	7.555	1.777	steady/unsteady
S130000	13.071	1.2266	101415	7.554	1.781	steady/unsteady
S140000	14.072	1.2263	101408	7.552	1.783	steady/unsteady
S150000	15.096	1.2240	101367	7.550	1.784	steady/unsteady

Table 1: Operational conditions in the FLUENT calculations.

The NREL Phase VI rotor is modelled without nacelle and tower to simplify the flow problem in FLUENT. Comparable conditions with negligible tower effects can only be found in the measurements of the first quarter of the upper half of the rotor plane (between azimuth angle of 0^o and

90°) and this data was used in the comparison. Blade vibrations and control intervening, as-well as variations in pressure distributions turned out to be smallest in this area [11, 12].

2.1. Computational mesh

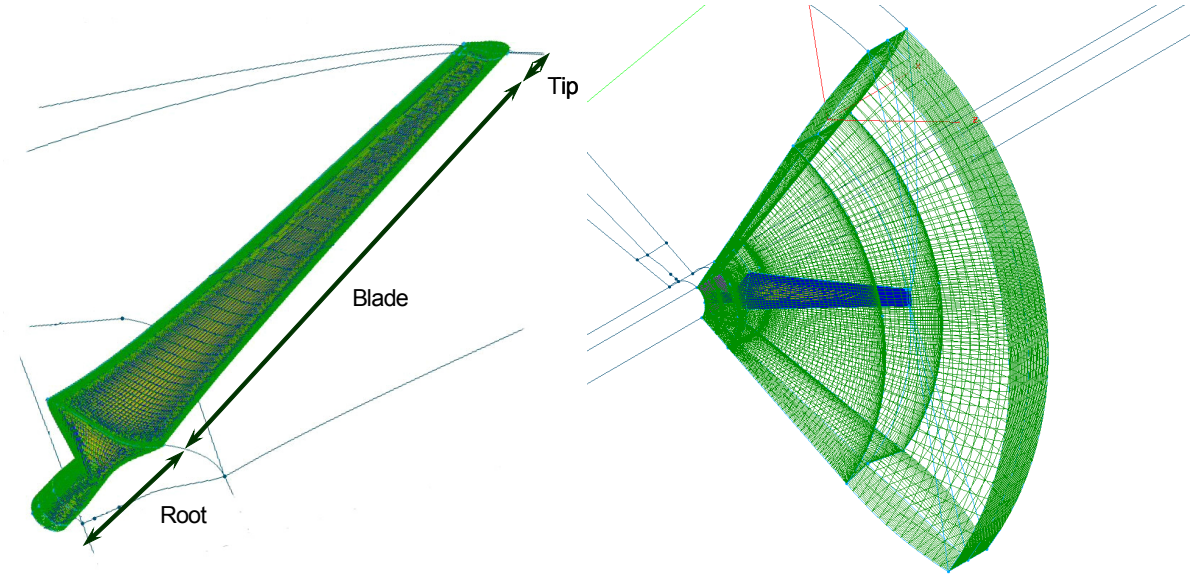

Figure 1. The boundary layer block (left) and the blocks immediately connected to this boundary layer block (right)

The computational model consists of one blade due to the 180° symmetry of the configuration. The mesh has 4 blocks with an O-O topology and starts around the blade. The blade mesh itself is subdivided in 3 parts; a root, blade and tip section. The first two parts have respectively 38 cells and 99 cells in span-wise direction and 196 cells wrapped around the cross profile. The tip has 39 cells along the span and only 61 cells around the cross sections. Figure 1 gives an impression of the cell distribution at the blade surface. From the blade surface a block is constructed to capture the thin boundary layer. The height of the first inner cell is equal to 4×10^{-2} mm and has y^+ of about one. The normal spacing has a growth rate of 1.2 and consists of 20 cells, this gives a cell amount in the boundary layer block of 0.5×10^6 cells. Around this block an O-O block is wrapped around covering a 90° azimuthal area. The block has 40 cells normal

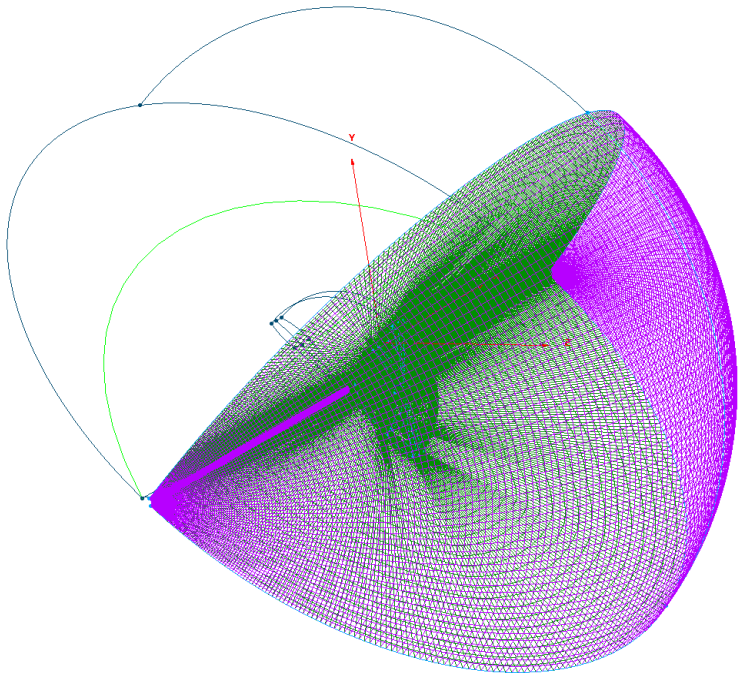

Figure 2. Overview of the domain with a dense spacing around the blade (block 3) and the remaining half (block 4)

to the blade and the length in span-wise direction is 1.5 radius. In total this block has 1.9×10^6 cells.

An outer block is constructed having the shape of a quarter sphere with a radius of 6 blade lengths. The outer block has 40 cells in radial direction and 61 in azimuthal direction, leading to a total of 0.7×10^6 cells. The computational domain is completed with a fourth block covering the remaining 90° and has 40 cells in azimuthal direction giving 0.6×10^6 cells (Fig. 2). The entire domain covers 180° in azimuthal direction and the four blocks contain a total of 3.6×10^6 cells.

2.2. Conditions

To model the rotating blade, the blade is put at a fixed position while the fluid is given a rotational reference frame. This approach prevents the need for sliding meshes. Furthermore the position of the blade is defined such that a great part of the wake, originating from the blade trailing edge, is captured directly in the computations. The blade geometry is placed at the bottom part 45° in azimuthal direction so the wake can be resolved over 135° before encountering the symmetry plane. It is believed that this blade position will improve solutions of the shedded vorticity in the wake. Full implicit periodic conditions are applied at the symmetry plane.

Upstream of the spherical domain the undisturbed wind speed is specified and this is treated as velocity inlet. This is 6 blade lengths away of the blade, just like the outlet. The latter is modeled as pressure outlet. At the center cylinder face slip conditions are applied, while the blade itself is modeled as a wall with no slip.

2.3. Turbulence models

The configurations start with an almost fully attached flow at the lowest tunnel speed of 8m/s and with increasing wind speeds parts of the flow separate and finally result in a fully separated flow along almost the entire blade span. Partly separated flows are commonly modelled with a k-ω SST eddy viscosity model while for huge separated areas the description of the detached eddy viscosity model, DES, is in general preferred. In this paragraph three options will be discussed at a wind speed of 13m/s:

- steady state solutions with the k-ω SST model
- unsteady computations with the k-ω SST model
- and computations with DES being unsteady.

All computations were fully turbulent and initialized with the robust k-ε turbulence model. After some 500 iterations the calculations were switched to the desired turbulence model. The steady computations already took approximately 2 days on a node of a workstation with 4 processors (3.8GHz) and 8GB of memory. The steady result was the start for the unsteady computations with a second order iterative time-stepping method. Time intervals of $1x10^{-4}$ second were chosen containing 20 iterations each. The latter was sufficient for a relatively nice periodical behavior per time interval.

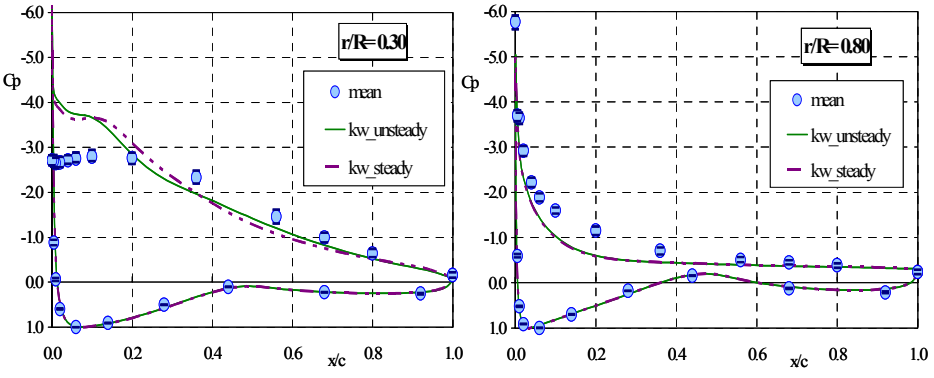

Figure 3. The effect of the steadiness of the k-ω SST model calculations for two span-wise locations compared with those of the UAE measurements at 13m/s tunnel speed. The error bars in the measurements represent the minimum and maximum measured Cp

This procedure was used for wind speeds of 12m/s and above.
The results at 13m/s are selected for detailed analysis and Fig. 3 shows the difference in CFD results for the steady and unsteady calculations with the k-ω SST model. The inboard segment at r/R=0.30 show the largest differences between the two calculations while these are almost negligible for the other segments and here represented by the 80% span location. For the unsteady result a representative mean value was taken. Variation (or amplitude) of the integrated loads were very small and close to one percent. This extreme small variation explains why almost all segments hardly show differences in outcome between steady and unsteady. This trend was representative for the other wind speeds as-well. Because in general predictions of the unsteady calculations of the inboard pressure distributions were slightly better, it was decided to use only these in the investigations.

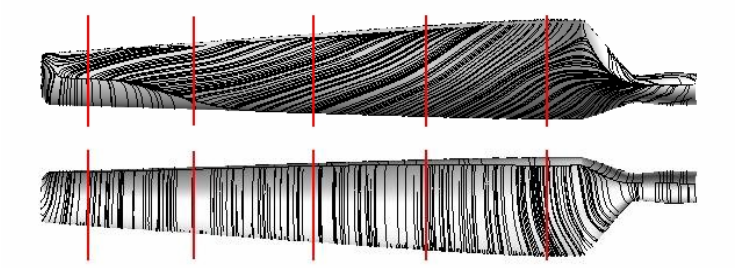

Figure 4. Limited streamlines on suction (upper) and pressure side with the k-ω model at 13m/s wind speed. The vertical lines indicate the segments at r/R= 0.95, 0.80, 0.63, 0.47 and 0.30

Figure 4 demonstrates the limited streamlines for this configuration and at the suction side turbulent separation starts almost immediately at the nose for the segments from mid-span to inboard (r/R= 0.63, 0.47 and 0.30). At 80% span turbulent separation begins at approximately 20% which position moves downstream to just after the 50% chord at the tip segment, r/R= 0.95. So from the calculations with the k-ω SST model it seems that 80 to 90% of the blade is exposed to the turbulent separated flow and it is then questionable if this turbulent model is still the most adequate one.

The detached eddy model is normally better adapted to largely separated flows and an (unsteady) FLUENT calculation was performed. Figure 5 shows the differences for 4 span segments between the measurements, the unsteady results with the k-ω SST model and DES. The differences between the k-ω and DES model are not that big and compared with the measurements the predictions with the k-ω model seem to be slightly better at most of the span locations. The predicted results at r/R= 0.30 are not very satisfactory for both models. The main reason is probably the insufficient characterization with the

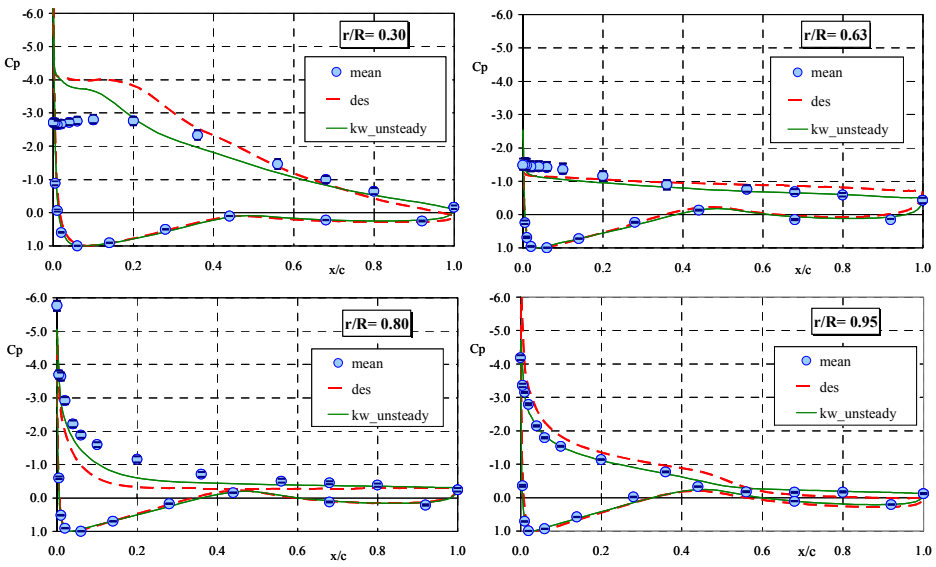

Figure 5. The effect of the unsteady k-ω SST and DES model on the pressure distributions compared with those of the measurements at 13m/s tunnel speed (DES is the dotted line)

turbulence model but some deviations could also be affected by uncertainty in the description of the shape between the largest chord and circular hub connection.

From these FLUENT results the best overall performance is obtained with the steady or unsteady k-ω SST model and this turbulence model will now be used in the determination of the section characteristics up till the wind speed of 15m/s.

3. Results and discussion

The rotor flow of the steady state non-yawed configuration will be analyzed for 8 wind speeds between 8m/s and 15m/s. At most of these wind speeds the flow over the airfoil is strongly exposed to cross flows caused by rotation. This results in augmented lift and stall delay and for this part of the characteristics many engineering methods were developed. These methods hardly include local blade shape and specific flow properties. With Navier-Stokes simulations all these issues are addressed and a few typical results will be highlighted. The k- ω SST results in the form of span wise pressure distributions at 10m/s and 15m/s will be discussed in detail. These wind speeds were also depicted by Sørensen [6] and enables some comparison between the commercial code FLUENT and the dedicated EllipSys3D code formulated by Risø and DTU.

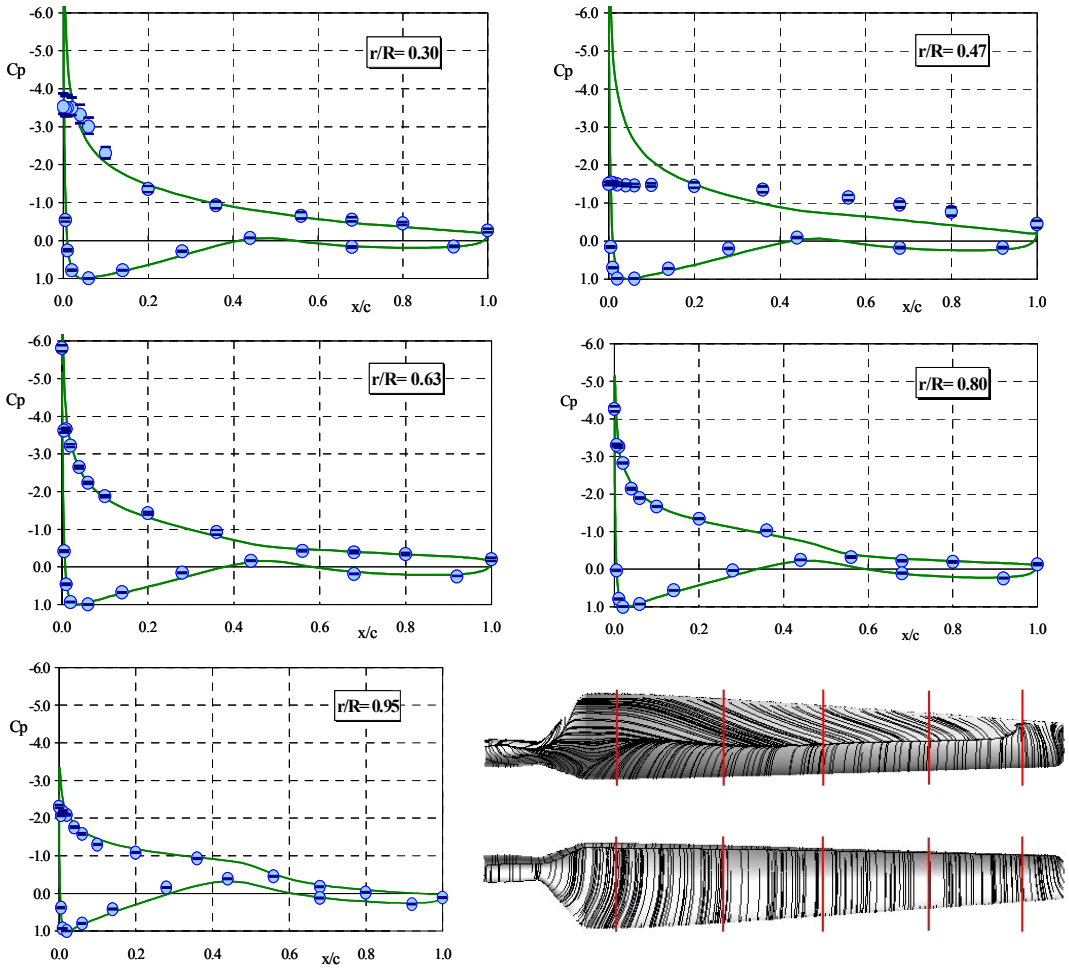

Figure 6. Pressure distributions for the 10m/s case plus the limited streamlines on suction (upper) and pressure side (Circles are measurements, full curve are steady k-ω SST. The error bars in the measurements represent the minimum and maximum measured Cp.)

3.1. Pressure distributions

Figure 6 displays the experimental and FLUENT results for 10m/s. The picture at the bottom right represents the limited streamlines and shows a partly separated flow at the suction side and a fully attached flow at the pressure side. At the suction side CFD predicts turbulent separation at approximately 40% chord for the inboard segment and this position moves downstream to about 60% chord at the outboard part. The span segment at r/R= 0.95 however is not exposed to turbulent separation and the flow seems to be fully attached up till the tip.

The measured values are from the UAE S-series a configuration with a clean blade without flow probes in front to minimize flow disturbances. The average values of the first rotor plane half, between 0^{o} and 90^{o} azimuth angle, is used as reference. The minimum and maximum values from the data points are given by horizontal lines and these can be observed in Fig. 6 as-well. Only at the inboard segment, r/R= 0.30, near the nose the minimum and maximum values in the measurements are outside the markers. This indicates unsteady flow behavior and large separated flow parts are the cause of this. Normally, separated flows are reflected as a horizontal part in the pressure distributions over the back of the airfoil (in particular in 2D). Cross flows disturb this and now a small pressure gradient is present

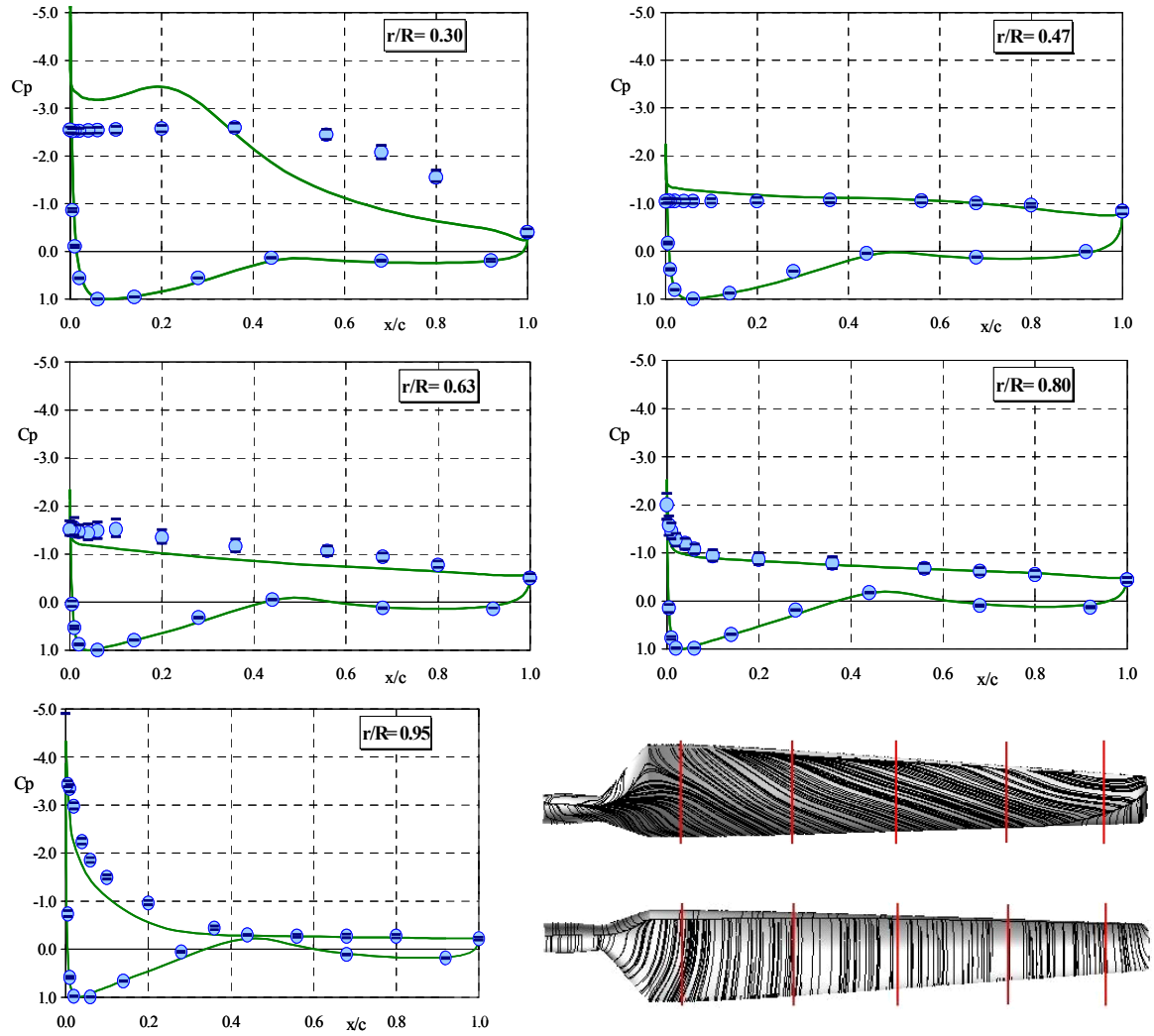

Figure 7. Pressure distributions for the 15m/s case plus the limited streamlines on suction (upper) and pressure side. (Circles are measurements, full curve are unsteady k-ω SST)

which is also the case in the CFD pressure distributions. Most of the calculated pressure distributions agree very well with the experimental data, except for the r/R= 0.47 segment. Here, calculations assume a partly attached flow over the front part of the profile while the measurements represent a pressure distribution of a fully separated flow. This particular case has been studied by e.g. J. Tangler and seems to be unique [13]. The behavior was attributed to a so called "standing" vortex. Towards outboard separation moves downstream and at the tip segment, r/R= 0.95, experimental and calculated pressure distributions show a fully attach flow and predictions are excellent.

The other results discussed here are at a wind speed of 15m/s and is displayed in Fig. 7. In this figure the graph with limited streamlines indicate that four of the five segments have a fully separated flow and cross flow is the dominant flow pattern at the suction side. At the tip, r/R= 0.95, turbulent separation occurs at approximately 25% from the chord leading edge. The difference in pressure distributions between measurements and FLUENT are largest at the inboard segment at r/R= 0.30 but is in reasonable agreement at the other segments. The predictions with the unsteady k- ω SST models seem to capture the flow fairly well, what is a bit surprising for fully separated flows. This is not the case at r/R= 0.30 and the FLUENT result is very poor.

At the pressure distributions with fully separated flow a strong and very small pressure peak at the nose can be observed. An increase of panels near the nose was investigated to reduce this but the peak was hardly affected and the most likely causes are numerical errors. No change in flow pattern could be detected.

The results shown here are fairly representative for the other investigated wind speeds and in general the predictions with FLUENT are surprisingly good. Two additional notes have to be made one with respect to the low wind speeds and another with the trend along the blade span. At wind speeds below 10m/s the separated flow part is less eminent and most of the flow is attached which gives the best predictions. Beyond 10 m/s turbulent separation moves quickly towards the nose and does this faster for the inboard than outboard sections with increasing wind speeds. This is the reason why the predictions at the inboard segments are sometimes poor but the results improve towards the tip.

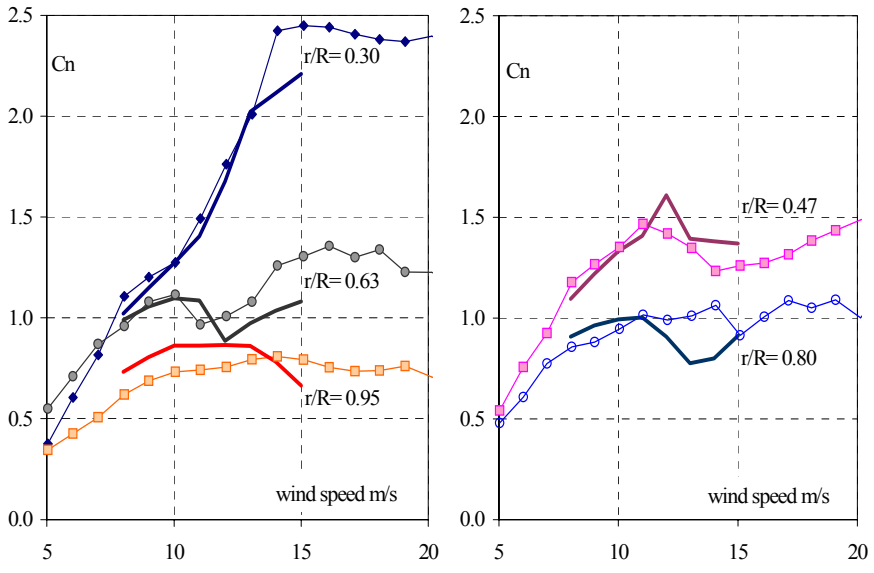

Figure 8. The normal force coefficient from the experiment and calculations per section (markers are measurements, full curves are k-ω SST)

3.2. Characteristics

Integrating the pressure distributions along the chord gives the normal force coefficient per segment and this was carried out for the UAE experiment (S-series) and the calculations. Figure 8 shows the normal force coefficient versus the wind speed. The difference in C_n per segment is sometimes considerable and the inboard segment at r/R= 0.30 turns out to be the best predicted with FLUENT. This is in contrast to what was observed from the

pressure distributions and differences along the chord seem to be cancelled out by integration. Despite the differences and the sometimes conflicting results, it is clear that the trends in normal force coefficients are followed. The largest coefficients are at the inboard segments and these values reduce towards the tip. The section at r/R= 0.80 is, in general, considered close to 2D and the values at the tip are at a much lower level.

Up till 11m/s four segments are predicted very well while comparison with the tip at r/R= 0.95 is poor. At increasing wind speeds deviation from the measurements become larger and this corresponds with an increase in separated flow. The relative large normal force coefficients at inboard and mid-span section will also be reflected in the lift values. To derive the lift coefficients an angle of attack is required in combination with the normal and tangential force coefficients. A proper inflow angle is not directly available and determination of it has very much to do with the definition. For convenience reasons it is decided to use the incidence from the UAE of a similar configuration as the S-series; the H-series. This approach has some uncertainties in angle-of-attack but it is expected that the effect on the CFD result will be small. Figure 9 shows the computations for the rotated blade compared with 2D measurements on the S809 airfoil [14]. The inboard segments r/R= 0.30 and r/R= 0.47 clearly show lift levels above what is obtained in 2D and augmented lift and delayed stall is confirmed. This increase is often attributed to radial pumping of the flow in the separated area and the strong cross flows in CFD demonstrate this. The segments at r/R= 0.63 and r/R= 80 show lift curves rather close to the 2D measurements and it seems that augmented lift due to rotation is not present at this part of the blade. The tip at r/R= 0.95 show a decrease of the maximum lift and losses due to finiteness of the blade cause this.

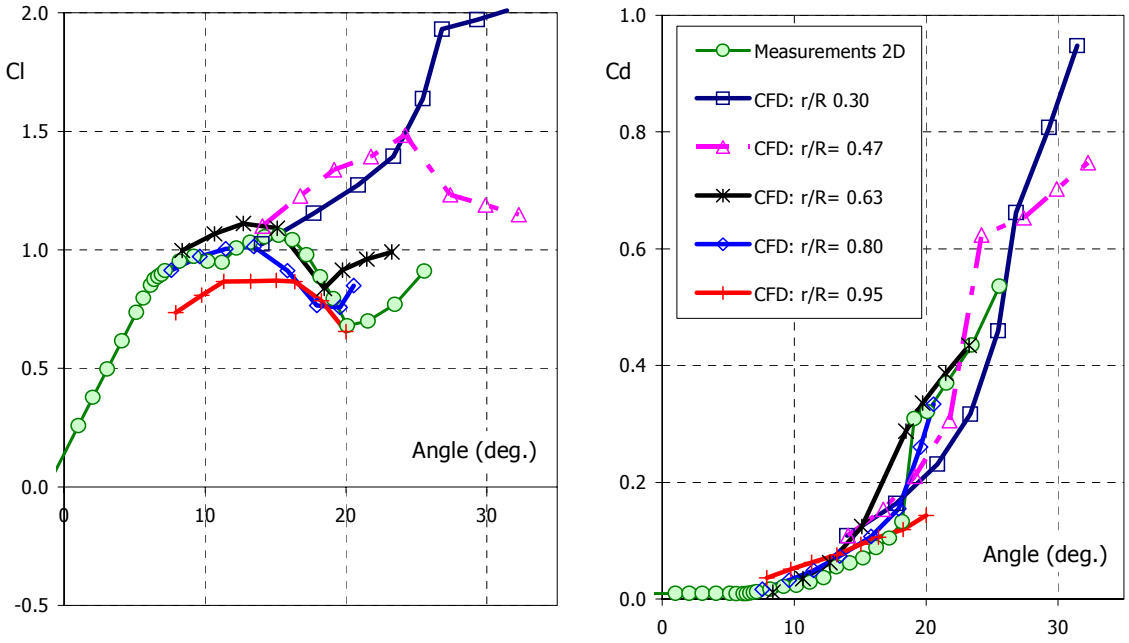

Figure 9. The difference between the FLUENT results due to rotation compared with the 2D S809 measurements. (The inflow angle is from the H-series of UAE)

The calculated drag between 15deg. and 25deg. wind around the measured drag with maximum deviation near 2D leading edge stall (at 19deg.). This holds for all segments. The sharp rise in the calculated drag beyond 25deg. could very well lead to drag values larger then measured but this can however not be establish here. There is unfortunately not a clear picture of the drag behavior for the rotating segments and more detailed investigations are needed. Assumptions of the inflow angle and the number of orifices at the profile nose could for instance play an important role.

4. Conclusions

A series of computations of the rotating NREL blade with the commercial code FLUENT have been performed. The configuration was similar to the non-yaw S-series measurements of the Unsteady Aerodynamic Experiment carried out in the NASA Ames wind tunnel. In the computations the standard k- ω SST turbulence model was preferred because the results were slightly better as the Detached Eddy Simulations. The influence of steady or unsteady computations turned out to be small, which is a bit amazing considering the unsteadiness of the hugely separated flow around the actual blade during the measurements. The computations show good agreement for almost all segments at wind speeds below 10m/s. The biggest deviations are at segment r/R= 0.47. Beyond 10m/s large areas of the blade are separated and cross flows dominate the limited streamlines. Deviations of the pressure distributions compared with the measurements are now larger in particular at the very inboard segment at r/R= 0.30, however the results for the other segments are surprisingly good.

To get around uncertainties in inflow angle C_n values are used in relation to the wind speeds. The trends of the measurements are followed by the calculations showing large normal force coefficients inboard and relative small values at the tip. The determination of lift confirm this and the segments at r/R= 0.30 and r/R= 0.47 clearly show augmented lift and stall delay as a consequence of rotation. The segments at r/R= 0.63 and r/R= 0.80 are close to the 2D measurements on the S809, while the tip part (r/R= 0.95) showed a strong reduction in lift compared to 2D.

The results of the drag are not convincing and some uncertainties could play a dominant role and further investigations are needed.

References

[1] Chaviaropoulos, PK, Hansen, MOL, “Investigating 3D and Rotational Effects on Wind Turbine Blades by Means of a Quasi-3D Navier-Stokes Solver”, ASME Journal of Fluids Engineering, Vol. 122, No.2, 200, pp 330-336

[2] Lindenburg, C., “Investigation into Rotor Blade Aerodynamics”, ECN-C--03-025, July, 2003

[3] Schepers, JG, Feigl, L, Rooij, van R, Bruining, A,” Analysis of Detailed Aerodynamic Field Measurements using Results from an Aeroelastic Code”, Wind Energy, Vol. 7, No. 4, pp 357-372

[4] Bak, C, Johansen, J, Andersen, P.B, ”Three-Dimensional Corrections of Airfoil Characteristics Based on Pressure Distributions”, Proceedings of the European Wind Energy Conference & Exhibition (EWEC), Feb.-Mar. 2006, Athens, Greece

[5] Hand MM, Simms DA, Fingersh LJ, Jager DW, Cotrell JR, Schreck S, Larwood SM, “Unsteady Aerodynamics Experiment Phase VI: Wind Tunnel Test Configurations and Available Data Campaigns”, December 2001, NREL/TP-500-29955

[6] Sørensen, NN, Michelsen, JA, Schreck, S, “Navier-Stokes Predictions of the NREL Phase VI Rotor in the NASA Ames 80ftx120ft Wind Tunnel”, Wind Energy, 2002, Vol. 5, pp 151-169

[7] Duque, EPN, Burklund, MD, Johnson, W, “Navier-Stokes Comprehensive Analysis Performance Predictions of the NREL Phase VI Experiment”, Journal of Solar Energy Engineering, November 2003, Vol. 125, pp 457-467

[8] Johansen, J, Sørensen, N.N, “Aerofoil Characteristics from 3D CFD Rotor Computations”, Wind Energy, Vol. 7, No. 4, pp 283-294

[9] Schmitz, S, Chattot, J-J, “Characterization of Three-Dimensional Effects for the Rotating and Parked NREL Phase VI Wind Turbine”, Journal of Solar Energy Engineering, November 2006, Vol. 128, pp 445-454

[10] Gonzalez, A, “Geometry and Rotational Effects on the Aerodynamic Behavior Using NREL UAE Data”, Proceedings of 45th AIAA Aerospace Sciences Meeting and Exhibit, Reno, USA, Januari-2007

[11] Kuik, GAM van, Rooij, RPJOM van, Imamura, H. “Analysis of the UAE phase VI wind tunnel results in the non-yawed flow”. Proceedings of the 2004 European Wind Energy Conference

and Exhibition on London, London, November-2004.

[12] Rooij, RPJOM van. "The effect of the test set-up on the steady state data". Proceedings of the 2005 Joint meeting of IEA R&D wind annex XI: Joint action on aerodynamics of wind turbines and IEA R&D wind annex XX: HAWT aerodynamics & models from wind tunnel measurements, Pamplona, Spain, May-2005

[13] Tangler, J.L, "Insight into a wind turbine stall and post-stall aerodynamics", Wind Energy, vol.7, Issue 3, pp 247-260.

[14] Somers, D.M, "Design and Experimental Results for the S809 Airfoil", Report NREL/SR-440-6918, Golden, CA, USA.